

COORDINATED CONTROL OF SATELLITES: THE ATTITUDE CASE

Thomas R. Krogstad
Department of Engineering Cybernetics,
Norwegian University of Science and Technology
N-7491 Trondheim, Norway
thomas.krogstad@itk.ntnu.no

Jan Tommy Gravdahl,
Department of Engineering Cybernetics,
Norwegian University of Science and Technology
N-7491 Trondheim, Norway
tommy.gravdahl@itk.ntnu.no

Raymond Kristiansen
Narvik University College
N-8505 Narvik, Norway
raymond.kristiansen@hin.no

Abstract—In this paper an observer-controller structure for attitude synchronization of a satellite formation is presented. The design applies methods from mechanical synchronization to design a nonlinear observer and controller for satellites actuated by means of reaction wheels and magnetic torquers. In this approach one satellite is defined as the leader of the formation, while the rest are defined as followers which synchronize their attitude with the leader. We apply the approach to the design of an coordinated attitude control scheme for a two-satellite formation. In addition we propose a momentum dumping scheme for satellites with redundant reaction wheel assemblies.

I. INTRODUCTION

The purpose of this paper is to derive a control scheme to synchronize the attitude of satellites orbiting in formation, in such a way that the satellites are able to keep their relative attitude in the presence of disturbances. The coordinated control of multiple agents in a formation environment is an area which has attracted much attention internationally in later years. The increased activity in the field, comes from a number of advantages; several small spacecraft may cooperate solving missions that would require one large spacecraft, functionality may be distributed to increase redundancy, the vehicles may be launched in stages on several launch vehicles, reducing the risk of total mission failure. The advantages do however come at the cost of a more complicated control system. Examples of current projects are Darwin, where six satellites will fly in tight formation to perform analysis of Earth-like planets, and MicroSAR, which are small low-cost SAR satellites capable of land and sea observations.

Noticeable contributions on formation control may be divided in to three separate approaches; leader-follower,

behavioural and virtual structure.

In the leader-follower strategy, one spacecraft is defined as the leader of the formation while the rest are defined as followers. The control objective is to enable the followers to keep a fixed relative attitude with respect to the leader [1]–[4].

The behavioural strategy views each vehicle of the formation as an agent and the control action for each agent is defined by a weighted average of the controls corresponding to each desired behaviour for the agent. This approach eases the implementation of conflicting or competing control objectives, such as tracking versus avoidance. It is however difficult to enforce group behaviour, and to mathematically guarantee stability and formation convergence. In addition, unforeseen behaviour may occur when goals are conflicting. This strategy is widely reported for use on mobile robots [5]–[7], and was also applied to spacecraft formations in [8].

In the virtual structure approach, the formation is defined as a virtual rigid body. In this approach the problem is how to define the desired attitude and position for each member of the formation such that the formation as a whole moves as a rigid body. In this scheme it is easy to prescribe a coordinated group behaviour and to maintain the formation during maneuvers. It is however dependent on the performance of the individual control systems of each member. This approach was used on mobile robots in [9] and more recently on spacecraft formations in [10], [11].

Stability analysis of both the observer and the synchronizing control scheme has been performed using an extension of a theorem due to Matrosov [12], given in [13]. This theorem proves to be very useful in the case of a semi-definite Lyapunov derivative when the analysed system is

time-varying, as for example in tracking control with a time-varying reference. In such a case the theorem usually referred to as LaSalle's invariance principle is not applicable.

A. Mechanical synchronization

The synchronization phenomenon describes the event when dynamical systems in some sense exhibit a similar behaviour in the time domain. In [14] some formal definitions were developed to describe the synchronization phenomenon, distinguishing between frequency and coordinate synchronization. Frequency synchronization describes the situation when the frequency of motion conforms to an integer multiple of a given frequency, ω_s , while coordinate synchronization occurs when the outputs or some state-variables of a system, coincide with the corresponding variables of some other system for all $t \geq 0$ or asymptotically as $t \rightarrow \infty$. In [4] coordinate synchronization was used in the synchronization of robot manipulators and in [15] it was proposed to use the theory in the replenishment and rendezvous of ships.

In this paper we adopt the problem formulation of [4], referred to as external synchronization. In this formulation we define a leader system, which is the dominant system, and a bounded set of follower systems. The synchronization problem consists of creating either physical interconnections or control feedback loops, which forces the outputs of the follower system to conform with those of the leader.

B. Electromagnetic actuators

Electromagnetic actuators are often chosen due to the independence of a limited fuel source, depending instead on power from solar arrays and batteries, thereby prolonging the lifespan of the mission. Electromagnetic actuators, often referred to as magnetic torquers, are based on two basic configurations. One is the coil based, where current is sent through a current loop which generates the magnetic moment proportional to the area of the coil and the number of windings. The other type is the magnetic rod, where a wire is wound around a rod made of a high permeability material. Both variations interact with the local geomagnetic field, generating a torque vector in the direction perpendicular to the magnetic moment and local field vectors.

C. Wheel actuators

A reaction wheel is essentially a torque providing motor with high rotor inertia. It is able to load and unload angular momentum internally, and is thus often referred to as a momentum exchange device, as it does not change the overall angular momentum of the satellite, but redistributes it to different parts. The amount of torque provided is dependent on the size of the rotor and motor, and is usually in the range from 0.01 Nm to 1 Nm.

A wheel complete with motor and drive electronics, is usually referred to as a reaction wheel assembly (RWA). Three wheels, one along each axis, is needed for full three-axis control. For redundancy and performance a composition of RWAs usually consists of more than three wheels. An

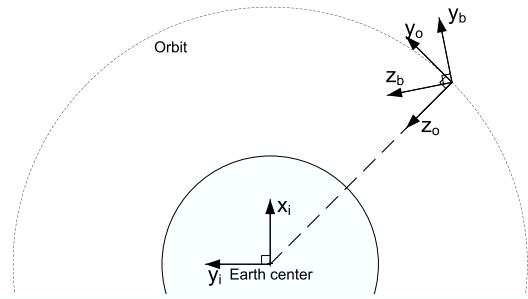


Fig. 1. Illustration of the reference frames for a satellite in equatorial orbit. The axes not shown are pointing out of the paper.

example is the tetrahedron composition. A regular tetrahedron is a pyramid composed of four equilateral triangular faces, three of which meet at each vertex. Each wheel-axis is placed orthogonal to a face, and meet at the center of the pyramid.

The torque from a wheel to the body equals the torque applied to the wheel from a motor attached to the body, but with opposite sign.

II. MODELLING

In this section, the model of a satellite actuated by means of reaction wheels and electromagnetic torquers is derived. The notation is based on [17] and [18].

A. Reference frames

When modelling the satellite, the equation of motion will be expressed in three different reference frames, illustrated in Fig. 1. A general reference frame will be denoted as \mathcal{F} with a subscript corresponding to a given frame.

1) *ECI - Earth-centered inertial frame*: This reference frame has its origin in the center of the Earth, the x_i -axis is pointing in the vernal equinox direction, Υ . This is in the direction of the vector from the center of the Sun through the center of the Earth during vernal equinox. The y_i -axis points 90° east, spanning the equatorial plane together with the x_i -axis. The z_i -axis points through the North Pole, completing the right-hand system. In the following this frame will be denoted by \mathcal{F}_i

2) *Orbit-fixed reference frame*: This frame, denoted \mathcal{F}_o , has its origin in the satellite's center of gravity. The z_o -axis points in the nadir direction. The y_o -axis points in the direction of the negative orbit normal. The x_o -axis is chosen as to complete a right-hand coordinate system.

3) *Body-fixed reference frame*: As the \mathcal{F}_o frame, this reference frame also has its origin in the satellite's center of gravity, with the axes pointing along the satellites principal axes of inertia. The frame is denoted \mathcal{F}_b . In the control design we denote the body frame of the leader and follower satellites as \mathcal{F}_l and \mathcal{F}_f respectively.

B. Kinematics

We describe the attitude kinematics in the form of Euler parameters, η and ϵ , which may be defined from the angle-

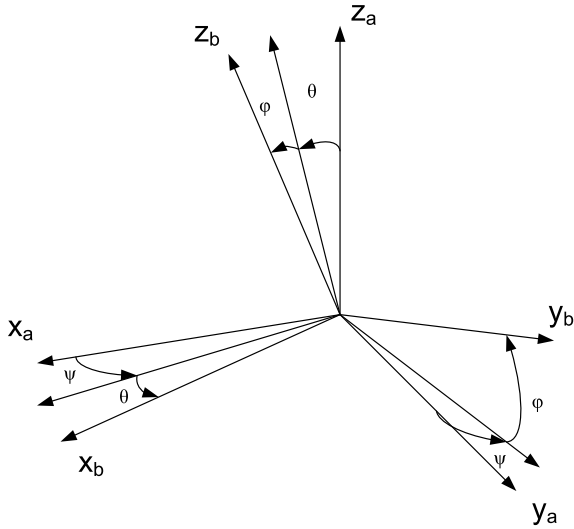


Fig. 2. The figure shows how the rotation between two frames can be interpreted in form of Euler angles.

axis parameters θ and \mathbf{k} as

$$\eta = \cos \frac{\theta}{2}, \quad \epsilon = \mathbf{k} \sin \frac{\theta}{2},$$

and which has the corresponding rotation matrix

$$\mathbf{R}(\eta, \epsilon) = \mathbf{1} + 2\eta\epsilon^\times + 2\epsilon^\times\epsilon^\times, \quad (1)$$

where \times denotes the vector cross product operator, and ϵ^\times is skew-symmetric. The choice of Euler parameters is motivated by their nonsingular properties. To describe a rotation between frames \mathcal{F}_a and \mathcal{F}_b , we use the notation η_{ab} and ϵ_{ab} . From the properties of the rotation matrix, it can be shown that the kinematic differential equation is

$$\dot{\mathbf{R}}_i^b = (\omega_{bi}^b)^\times \mathbf{R}_i^b = -(\omega_{ib}^b)^\times \mathbf{R}_i^b, \quad (2)$$

where ω_{bi}^b is the angular velocity of the body frame \mathcal{F}_b with respect to the inertial frame \mathcal{F}_i , and \mathbf{R}_i^b is the rotation matrix between frames.

Using (1) and (2) the kinematic differential equations

$$\dot{\eta}_{ib} = -\frac{1}{2}\epsilon_{ib}^T \omega_{ib}^b \quad (3a)$$

$$\dot{\epsilon}_{ib} = \frac{1}{2}[\eta_{ib}\mathbf{I} + \epsilon_{ib}^\times]\omega_{ib}^b, \quad (3b)$$

can be derived. Given the quaternion vector

$$\mathbf{q}_{ib} \triangleq \begin{bmatrix} \eta_{ib} \\ \epsilon_{ib} \end{bmatrix}, \quad (4)$$

we may write the (3) in compact form

$$\dot{\mathbf{q}}_{ib} = \frac{1}{2}\mathbf{Q}(\mathbf{q}_{ib})\omega_{ib}^b, \quad (5)$$

where

$$\mathbf{Q}(\mathbf{q}_{ib}) \triangleq \begin{bmatrix} -\epsilon_{ib}^T \\ \eta_{ib}\mathbf{I}_{3 \times 3} + \epsilon_{ib}^\times \end{bmatrix} \quad (6)$$

Euler angles, or roll-pitch-yaw angles, have been applied in the visualization of results, since these are easier to relate to physical motion. Fig. 2 illustrates a rotation from \mathcal{F}_a to \mathcal{F}_b in Euler angles.

C. Dynamics

A satellite actuated by means of reaction wheels, may be modelled as a rigid body in combination with several rotors or wheels, commonly referred to as a gyrostat [17].

We start by writing the total angular momentum of the gyrostat in \mathcal{F}_b and the total axial angular momentum of the wheels

$$\mathbf{h}^b = \mathbf{J}\omega_{ib}^b + \mathbf{A}\mathbf{I}_s\omega_s \quad (7a)$$

$$\mathbf{h}_a = \mathbf{I}_s\mathbf{A}^T\omega_{ib}^b + \mathbf{I}_s\omega_s, \quad (7b)$$

where $\mathbf{A} \in \mathbb{R}^{3 \times 4}$ is a matrix of wheel axes in \mathcal{F}_b given by, [16],

$$\mathbf{A} = \begin{bmatrix} \sqrt{\frac{1}{3}} & \sqrt{\frac{1}{3}} & -\sqrt{\frac{1}{3}} & -\sqrt{\frac{1}{3}} \\ \sqrt{\frac{2}{3}} & -\sqrt{\frac{2}{3}} & 0 & 0 \\ 0 & 0 & -\sqrt{\frac{2}{3}} & \sqrt{\frac{2}{3}} \end{bmatrix}, \quad (8)$$

$\mathbf{I}_s \in \mathbb{R}^{4 \times 4}$ a diagonal matrix of wheel axial inertias, $\omega_s \in \mathbb{R}^4$ a vector of wheel velocities and $\mathbf{J} \in \mathbb{R}^{3 \times 3}$ the total moment of inertia.

Assuming that the body system coincides with the center of mass, we may obtain an expression for the change of angular momentum as

$$\dot{\mathbf{h}}^b = (\mathbf{h}^b)^\times \bar{\mathbf{J}}^{-1}(\mathbf{h}^b - \mathbf{A}\mathbf{h}_a) + \tau_e^b \quad (9a)$$

$$\dot{\mathbf{h}}_a = \tau_a, \quad (9b)$$

where $\bar{\mathbf{J}} \in \mathbb{R}^{3 \times 3}$ is an inertia-like matrix defined as

$$\bar{\mathbf{J}} \triangleq \mathbf{J} - \mathbf{A}\mathbf{I}_s\mathbf{A}^T$$

and τ_e^b is the resultant external torques due to magnetic control and environmental disturbances

$$\tau_e^b = \tau_m^b + \tau_g^b + \tau_d^b, \quad (10)$$

where τ_d^b is a vector of unknown disturbance torques, and τ_m^b and τ_g^b are magnetic control torques and gravitational disturbance torques, respectively, given by

$$\tau_g^b = 3\omega_0^2(\mathbf{z}_{o3}^b)^\times \mathbf{J}\mathbf{z}_{o3}^b \quad (11)$$

$$\tau_m^b = (\mathbf{m}^b)^\times \mathbf{B}^b(t), \quad (12)$$

where ω_0 is the orbital rotation rate, \mathbf{z}_{o3}^b is the Earth pointing vector, \mathbf{m}^b is the magnetic moment generated by the actuators and $\mathbf{B}^b(t)$ is the local geomagnetic field vector. The gravitational torque model given assumes a circular orbit.

Equation (9) may also be expressed in terms of angular velocities as

$$\mathbf{J}\dot{\omega}_{ib}^b = (\mathbf{J}\omega_{ib}^b)^\times \omega_{ib}^b + (\mathbf{A}\mathbf{I}_s\omega_s)^\times \omega_{ib}^b - \mathbf{A}\tau_a + \tau_e \quad (13a)$$

$$\mathbf{I}_s\dot{\omega}_s = \tau_a - \mathbf{I}_s\mathbf{A}\dot{\omega}_{ib}^b \quad (13b)$$

III. CONTROL DESIGN

A group of satellites are assumed synchronized when the relative attitude deviation and angular velocity between the leader and the follower(s) approaches zero asymptotically as $t \rightarrow \infty$. In our design, the relative attitude deviation or synchronization error, is represented by the quaternion error

$$\mathbf{q}_{se} \triangleq \mathbf{q}_{lf} = \mathbf{q}_{li} \otimes \mathbf{q}_{if} = \mathbf{q}_{li}^{-1} \otimes \mathbf{q}_{if}, \quad (14)$$

while the angular velocity synchronization error is equal to the relative velocity,

$$\boldsymbol{\omega}_{se} \triangleq \boldsymbol{\omega}_{lf}^f = \boldsymbol{\omega}_{if}^f - \mathbf{R}_l^f \boldsymbol{\omega}_{il}^l. \quad (15)$$

Further we assume that the leader satellite is controlled by a stable or asymptotically stable control law. The problem is then to design a controller for the follower which synchronizes the attitude.

Given the error-variables (14) and (15), the error-dynamics may be represented by

$$\begin{aligned} \mathbf{J}\dot{\boldsymbol{\omega}}_{se} &= (\mathbf{J}\boldsymbol{\omega}_{if}^f + \mathbf{A}\mathbf{I}_s\boldsymbol{\omega}_{s,f})^\times \boldsymbol{\omega}_{if}^f - \mathbf{A}\boldsymbol{\tau}_{a,f} + \boldsymbol{\tau}_{g,f} \\ &\quad - \mathbf{J}(\boldsymbol{\omega}_{se})^\times \mathbf{R}_l^f \boldsymbol{\omega}_{il}^l - \mathbf{J}\mathbf{R}_l^f \dot{\boldsymbol{\omega}}_{il}^l \end{aligned} \quad (16a)$$

$$\dot{\mathbf{q}}_{se} = \frac{1}{2}\mathbf{Q}(\mathbf{q}_{se})\boldsymbol{\omega}_{se}, \quad (16b)$$

where the subscripts f on $\boldsymbol{\tau}_{a,f}$ and $\boldsymbol{\tau}_{g,f}$, is to clearly distinguish between leader and follower torques.

The following proposition gives a model-dependant controller for the external synchronization of the satellites

Proposition 1. *The error-dynamics (16), with control input given by*

$$\begin{aligned} \boldsymbol{\tau}_{a,f} &= -\mathbf{A}^\dagger \left\{ -(\mathbf{J}\boldsymbol{\omega}_{if}^f + \mathbf{A}\mathbf{I}_s\boldsymbol{\omega}_{s,f})^\times \mathbf{R}_l^f \boldsymbol{\omega}_{il}^l - \boldsymbol{\tau}_{g,f} \right. \\ &\quad \left. + \mathbf{J}(\boldsymbol{\omega}_{se})^\times \mathbf{R}_l^f \boldsymbol{\omega}_{il}^l + \mathbf{J}\mathbf{R}_l^f \dot{\boldsymbol{\omega}}_{il}^l \right. \\ &\quad \left. - k_d\boldsymbol{\omega}_{se} + k_p \text{sgn}(\eta_{se})\boldsymbol{\epsilon}_{se} \right\}, \end{aligned} \quad (17)$$

have a uniformly globally asymptotically stable origin $(\boldsymbol{\omega}_{se}, \mathbf{y}) = (\mathbf{0}, \mathbf{0})$, where $\mathbf{y} \triangleq \text{col}(1 - |\eta_{se}|, \boldsymbol{\epsilon}_{se})$

Proof. We prove the proposition using Theorem 2, which can be found in the Appendix.

Satisfying Assumption 1

Choosing the Lyapunov function

$$V = \frac{1}{2}\boldsymbol{\omega}_{se}^T \mathbf{J}\boldsymbol{\omega}_{se} + k_p \mathbf{y}^T \mathbf{y}, \quad (18)$$

the time-derivative along the trajectories of (16) can be found as

$$\dot{V} = \boldsymbol{\omega}_{se}^T \mathbf{J}\dot{\boldsymbol{\omega}}_{se} + k_p \text{sgn}(\eta_{se})\boldsymbol{\epsilon}_{se}^T \boldsymbol{\omega}_{se} \quad (19)$$

$$= \boldsymbol{\omega}_{se}^T \left[k_p \text{sgn}(\eta_{se})\boldsymbol{\epsilon}_{se} - (\mathbf{J}\boldsymbol{\omega}_{il}^l + \mathbf{A}\mathbf{I}_s\boldsymbol{\omega}_{s,l})^\times \boldsymbol{\omega}_{il}^l \right. \quad (20)$$

$$\left. + \mathbf{A}\boldsymbol{\tau}_{a,f} - \boldsymbol{\tau}_{g,f} + \mathbf{J}(\boldsymbol{\omega}_{se})^\times \mathbf{R}_l^f \boldsymbol{\omega}_{il}^l + \mathbf{J}\mathbf{R}_l^f \dot{\boldsymbol{\omega}}_{il}^l \right]. \quad (21)$$

Inserting for (17), results in

$$\dot{V} = -k_d\boldsymbol{\omega}_{se}^T \boldsymbol{\omega}_{se} \leq 0. \quad (22)$$

Which guarantees UGS for the error-dynamics (16), satisfying Assumption 1.

Remark 1. *From this result it is possible to show asymptotic convergence as in [19], by using Barbalat's lemma, and prove that convergence of $\boldsymbol{\omega}_{se}$ leads to convergence of $\boldsymbol{\epsilon}_{se}$.*

Satisfying Assumption 2

Since the origin is UGS, $\dot{\boldsymbol{\omega}}_{se}$, $\boldsymbol{\omega}_{se}$, \mathbf{y} are bounded functions of time. For $i = 1$ we choose

$$V_1 \triangleq V \quad (23)$$

$$\phi_1 \triangleq 0 \quad (24)$$

$$Y_1 \triangleq -\beta\|\boldsymbol{\omega}_{se}\| \leq 0 \quad (25)$$

V_1 is continuously differentiable and bounded, ϕ_1 is continuous and bounded, and finally Y_1 is continuous and hence assumption 2 is satisfied for $i = 1$.

For $i = 2$, we choose

$$V_2 \triangleq \boldsymbol{\omega}_{se}^T \mathbf{J}\boldsymbol{\epsilon}_{se} \eta_{se} \quad (26)$$

$$\phi_2 \triangleq \dot{\boldsymbol{\omega}}_{se} \quad (27)$$

$$Y_2 \triangleq \eta_{se}\phi_2^T \mathbf{J}\boldsymbol{\epsilon}_{se} + \eta_{se}\boldsymbol{\omega}_{se}^T \mathbf{J}\dot{\boldsymbol{\epsilon}}_{se} + \eta_{se}^T \mathbf{J}\boldsymbol{\epsilon}_{se} \quad (28)$$

Since $\dot{\boldsymbol{\omega}}_{se}$, $\boldsymbol{\omega}_{se}$, \mathbf{y} , $\dot{\eta}_{se}$ are bounded functions of time, V_2 , ϕ_2 and Y_2 are bounded. Moreover, V_2 is continuously differentiable, and ϕ_2 and Y_2 are continuous in their arguments. Hence, Assumption 2 is satisfied for $i = 2$.

Satisfying Assumption 3

$Y_1 \leq 0$ for all $\boldsymbol{\omega}_{se} \in \mathbb{R}^3$, satisfying Assumption 3 for $i = 1$. Moreover,

$$Y_1 = 0 \Rightarrow \|\boldsymbol{\omega}_{se}\| = 0 \Rightarrow Y_2 = \eta_{se}\phi_2^T \mathbf{J}\boldsymbol{\epsilon}_{se} \quad (29)$$

Inserting for ϕ_2 and $\boldsymbol{\omega}_{se} = 0$, gives

$$Y_2 = -k_p \eta_{se} \text{sgn}(\eta_{se})\boldsymbol{\epsilon}_{se}^T \boldsymbol{\epsilon}_{se} = -k_p |\eta_{se}| \boldsymbol{\epsilon}_{se}^T \boldsymbol{\epsilon}_{se} \leq 0. \quad (30)$$

Thus, Assumption 3 has been satisfied for both $i \in \{1, 2\}$.

Satisfying Assumption 4

It can now be seen that

$$\{Y_1 = 0, Y_2 = 0\} \Rightarrow \boldsymbol{\omega}_{se} = 0, \boldsymbol{\epsilon}_{se} = 0 \Rightarrow 1 - |\eta_{se}| = 0, \quad (31)$$

satisfying Assumption 4 for $i \in \{1, 2\}$.

Remark 2. *This hold as long as η_{se} is different from zero. Using UGS property of Assumption 1 and that $\eta_{se} = 0$ is an unstable equilibrium point when using the given definition of signum, as shown in [19], the condition is met by requiring η_{se} to initially be different from 0.*

The assumptions of Theorem 2 are satisfied, and we may conclude *uniform global asymptotic stability* of the synchronization error dynamics. \square

IV. OBSERVER DESIGN

Assuming only attitude is available for measurement, an observer is needed to estimate angular velocities and accelerations. Both an extended Kalman filter and a nonlinear observer are possible choices. In this paper a nonlinear observer is designed, but the interested reader is referred to [20] for a thorough review of the extended Kalman filter for satellite application.

Rewriting the dynamics in the inertial frame

$$\dot{\mathbf{h}}^i = \boldsymbol{\tau}_e^i = \mathbf{R}_b^i \boldsymbol{\tau}_e^b \quad (32a)$$

$$\boldsymbol{\omega}_{ib}^b = (\mathbf{R}_b^i \mathbf{J})^{-1} (\mathbf{h}^i - \mathbf{A} \mathbf{I}_s \boldsymbol{\omega}_s) \quad (32b)$$

$$\dot{\mathbf{q}}_{ib} = \frac{1}{2} \mathbf{Q}(\mathbf{q}_{ib}) \boldsymbol{\omega}_{ib}^b, \quad (32c)$$

we may define the observer as a copy of the dynamics including output injection terms as

$$\dot{\hat{\mathbf{h}}}^i = \boldsymbol{\tau}_e^i = \mathbf{R}_b^i (\boldsymbol{\tau}_e^b + \mathbf{g}_1(\mathbf{q}_{ib}, \hat{\mathbf{q}}_{ib})) \quad (33a)$$

$$\dot{\hat{\boldsymbol{\omega}}}_{ib}^b = (\mathbf{R}_b^i \mathbf{J})^{-1} (\hat{\mathbf{h}}^i - \mathbf{A} \mathbf{I}_s \boldsymbol{\omega}_s) \quad (33b)$$

$$\dot{\hat{\mathbf{q}}}_{ib} = \frac{1}{2} \mathbf{Q}(\hat{\mathbf{q}}_{ib}) (\hat{\boldsymbol{\omega}}_{ib}^b + \mathbf{g}_2(\mathbf{q}_{ib}, \hat{\mathbf{q}}_{ib})), \quad (33c)$$

where \mathbf{g}_1 and \mathbf{g}_2 are to be defined. Given the error variables

$$\tilde{\mathbf{h}}^i \triangleq \mathbf{h}^i - \hat{\mathbf{h}}^i \quad (34)$$

$$\tilde{\mathbf{q}}_{ib} \triangleq \mathbf{q}_{ib} \otimes \hat{\mathbf{q}}_{ib}, \quad (35)$$

the resulting error-dynamics may be written as

$$\dot{\tilde{\mathbf{h}}}^i = -\mathbf{g}_1(\mathbf{q}_{ib}, \hat{\mathbf{q}}_{ib}) \quad (36a)$$

$$\dot{\tilde{\eta}}_{ib} = -\frac{1}{2} \tilde{\boldsymbol{\epsilon}} (\boldsymbol{\omega}_{ib}^b - \hat{\boldsymbol{\omega}}_{ib}^b - \mathbf{g}_2(\mathbf{q}_{ib}, \hat{\mathbf{q}}_{ib})) \quad (36b)$$

$$\dot{\tilde{\boldsymbol{\epsilon}}}_{ib} = \frac{1}{2} (\eta \mathbf{I}_{3 \times 3} + \mathbf{S}(\tilde{\boldsymbol{\epsilon}})) (\boldsymbol{\omega}_{ib}^b - \hat{\boldsymbol{\omega}}_{ib}^b - \mathbf{g}_2(\mathbf{q}_{ib}, \hat{\mathbf{q}}_{ib})). \quad (36c)$$

Proposition 2. *The observer given by (33a)-(33c), with error dynamics (36a)-(36c), has an uniformly globally asymptotically stable origin $(\tilde{\mathbf{h}}, \tilde{\boldsymbol{\epsilon}}, \tilde{\eta}) = (\mathbf{0}, \mathbf{0}, \pm 1)$ if the output injection terms are chosen as:*

$$\mathbf{g}_1(\mathbf{q}_{ib}, \hat{\mathbf{q}}_{ib}) = -k_p \frac{dH(\tilde{\eta})}{d\tilde{\eta}} \mathbf{R}_b^i \mathbf{J}^{-1} \tilde{\boldsymbol{\epsilon}} \quad (37)$$

$$\mathbf{g}_2(\mathbf{q}_{ib}, \hat{\mathbf{q}}_{ib}) = -k_v \frac{dH(\tilde{\eta})}{d\tilde{\eta}} \tilde{\boldsymbol{\epsilon}}, \quad (38)$$

where $H(\cdot)$ is scalar function satisfying

- $H(\cdot) : [-1; 1] \rightarrow \mathbb{R}_+$ (non-negative)
- $H(-1) = 0$ or/and $H(1) = 0$
- $H(\cdot)$ is Lipschitz on $[-1, 1]$:

$$|H(\eta_1) - H(\eta_2)| \leq L |\eta_1 - \eta_2| \quad (39)$$

Several suggestions of $H(\tilde{\eta})$ were made in [19], and in this paper it is chosen to be

$$H(\tilde{\eta}) \triangleq \text{sgn}(\tilde{\eta}) \quad (40)$$

Proof. To prove proposition 2 the generalized Matrosov theorem, given in this work as Theorem 2, will be applied.

Satisfying Assumption 1

To prove that the origin of (36a)-(36c) is uniformly globally stable (UGS), we propose the Lyapunov function candidate

$$V_{obs} = \frac{1}{2} (\tilde{\mathbf{h}}^i)^T \tilde{\mathbf{h}}^i + 2k_p H(\tilde{\eta}) \quad (41)$$

as given in [19]. We find the derivative of (41) along the trajectories as

$$\begin{aligned} \dot{V}_{obs} &= (\tilde{\mathbf{h}}^i)^T \dot{\tilde{\mathbf{h}}}^i + 2k_p \frac{dH(\tilde{\eta})}{d\tilde{\eta}} \dot{\tilde{\eta}} \\ &= -(\tilde{\mathbf{h}}^i)^T (\mathbf{g}_1(\mathbf{q}_{ib}, \hat{\mathbf{q}}_{ib}) + k_p \frac{dH(\tilde{\eta})}{d\tilde{\eta}} (\mathbf{R}_b^i \mathbf{J}^{-1}) \tilde{\boldsymbol{\epsilon}}) \\ &\quad + k_p \frac{dH(\tilde{\eta})}{d\tilde{\eta}} \tilde{\boldsymbol{\epsilon}}^T \mathbf{g}_2(\mathbf{q}_{ib}, \hat{\mathbf{q}}_{ib}). \end{aligned} \quad (42)$$

Selecting the output injection terms \mathbf{g}_1 and \mathbf{g}_2 as

$$\mathbf{g}_1(\mathbf{q}_{ib}, \hat{\mathbf{q}}_{ib}) \triangleq -k_p \frac{dH(\tilde{\eta})}{d\tilde{\eta}} \mathbf{R}_b^i \mathbf{J}^{-1} \tilde{\boldsymbol{\epsilon}} \quad (44)$$

$$\mathbf{g}_2(\mathbf{q}_{ib}, \hat{\mathbf{q}}_{ib}) \triangleq -k_v \frac{dH(\tilde{\eta})}{d\tilde{\eta}} \tilde{\boldsymbol{\epsilon}}, \quad (45)$$

we obtain

$$\dot{V}_{obs} = -k_p k_v \left(\frac{dH(\tilde{\eta})}{d\tilde{\eta}} \right)^2 \tilde{\boldsymbol{\epsilon}}^T \tilde{\boldsymbol{\epsilon}} \leq 0. \quad (46)$$

Thus we have fulfilled the requirements of Theorem 1, and we can conclude that the origin is uniformly globally stable, UGS.

Satisfying Assumption 2

Since the origin is UGS, $\tilde{\mathbf{h}}, \tilde{\boldsymbol{\epsilon}}, \tilde{\eta}$ and $\dot{\tilde{\eta}}$ are bounded functions of time. For $i = 1$ we choose

$$V_1 \triangleq V_{obs} \quad (47)$$

$$\phi_1 \triangleq 0 \quad (48)$$

$$Y_1 \triangleq -\beta \|\tilde{\boldsymbol{\epsilon}}\|^2 \leq 0 \quad (49)$$

The function V_1 is continuously differentiable and bounded, ϕ_1 is continuous and bounded and finally Y_1 is continuous and hence assumption 2 is satisfied for $i = 1$.

For $i = 2$, we choose

$$V_2 \triangleq -\tilde{\eta} \tilde{\boldsymbol{\epsilon}}^T (\mathbf{R}_b^i \mathbf{J}) \tilde{\mathbf{h}} \quad (50)$$

$$\phi_2 \triangleq \dot{\tilde{\eta}} \quad (51)$$

$$Y_2 \triangleq -\dot{\tilde{\eta}} \tilde{\boldsymbol{\epsilon}}^T (\mathbf{R}_b^i \mathbf{J}) \tilde{\mathbf{h}} - \tilde{\eta} \dot{\tilde{\boldsymbol{\epsilon}}}^T (\mathbf{R}_b^i \mathbf{J}) \tilde{\mathbf{h}} \quad (52)$$

$$- \tilde{\eta} \tilde{\boldsymbol{\epsilon}}^T (\dot{\mathbf{R}}_b^i \mathbf{J}) \tilde{\mathbf{h}} - \tilde{\eta} \tilde{\boldsymbol{\epsilon}}^T (\mathbf{R}_b^i \mathbf{J}) \dot{\tilde{\mathbf{h}}} \quad (53)$$

Since $\tilde{\mathbf{h}}, \dot{\tilde{\mathbf{h}}}, \tilde{\boldsymbol{\epsilon}}, \dot{\tilde{\boldsymbol{\epsilon}}}$ and $\tilde{\eta}$ are bounded functions of time, V_2 , ϕ_2 and Y_2 are bounded. Moreover, V_2 is continuously differentiable and ϕ_2 and Y_2 are continuous in their arguments. Hence, assumption 2 is satisfied for $i = 2$.

Satisfying assumption 3

The function $Y_1 \leq 0$ for all $\tilde{\boldsymbol{\epsilon}} \in \mathbb{R}^3$. Hence assumption 3 is satisfied for $i = 1$. Moreover,

$$Y_1 = 0 \Rightarrow \|\tilde{\boldsymbol{\epsilon}}\| = 0 \Rightarrow Y_2 = -\tilde{\eta} \phi_2^T (\mathbf{R}_b^i \mathbf{J}) \tilde{\mathbf{h}} \quad (54)$$

Inserting for ϕ_2 and $-\tilde{\epsilon} = 0$, gives

$$Y_2 = -\tilde{\eta} \left[\frac{1}{2} (\tilde{\eta} (\mathbf{R}_b^i \mathbf{J})^{-1} \tilde{\mathbf{h}})^T (\mathbf{R}_b^i \mathbf{J}) \tilde{\mathbf{h}} \right] \quad (55)$$

$$= -\frac{1}{2} \tilde{\eta}^2 \tilde{\mathbf{h}}^T \tilde{\mathbf{h}} \quad (56)$$

$$= -\frac{1}{2} \tilde{\mathbf{h}}^T \tilde{\mathbf{h}} \leq 0, \quad (57)$$

where we have used that $\tilde{\epsilon} = 0 \Rightarrow \tilde{\eta} = \pm 1$. This shows that Assumption 3 is satisfied for $i = 2$.

Satisfying assumption 4

It is clear that

$$\{Y_1 = 0, Y_2 = 0\} \Rightarrow \|\tilde{\mathbf{h}}\| = 0, \|\tilde{\epsilon}\| = 0, \tilde{\eta} = \pm 1 \quad (58)$$

and thus assumption 4 is satisfied for $i \in \{1, 2\}$.

We have verified all the assumptions of Theorem 2, and we conclude that the origin $(\tilde{\mathbf{h}}, \tilde{\epsilon}, \tilde{\eta}) = (0, 0, \pm 1)$ is *uniformly globally asymptotically stable*. \square

V. MOMENTUM DUMPING SCHEME

Due to disturbances on the spacecraft, which are non-symmetrical over the orbit, angular momentum will build up in the reaction wheels. Thus their speed will increase, and eventually saturate as the maximum wheel speed is reached. When a wheel saturates, it cannot produce a torque in the direction which requires an increase of speed. To desaturate the wheels and dump the excess momentum, some form of external torque must be applied. Typically either from thrusters or magnetic torquers. In this paper we have used the latter, due to the independence of an expendable fuel source.

The magnetic torquers produce a torque vector given by (12). This relation is non-invertable, due to the skew-symmetric property of $(\mathbf{B}^b)^\times$, hence it is not possible to specify the magnetic moment which results in a desired torque. In fact the only feasible torques belongs to the space of vectors which is perpendicular to the geomagnetic field vector, which is a 2-dimensional manifold in \mathbb{R}^3 . We therefor follow the approach of [21], and project the ideal torque vector onto the space of possible vectors and get the relation

$$\boldsymbol{\tau}_m = \boldsymbol{\tau}_{m,\text{ideal}} - \Delta \boldsymbol{\tau}_m, \boldsymbol{\tau}_m \in \{\boldsymbol{\tau}_m \in \mathbb{R}^3 | \boldsymbol{\tau}_m \perp \mathbf{B}^b\} \quad (59)$$

where $\Delta \boldsymbol{\tau}_m$ is given by

$$\Delta \boldsymbol{\tau}_m = \frac{(\mathbf{B}^b)^\times \boldsymbol{\tau}_{m,\text{ideal}}}{\|\mathbf{B}^b\|^2} \quad (60)$$

Following the approach in [22], we select the magnetic moment according to

$$\mathbf{m}^b = -\frac{1}{\|\mathbf{B}^b(t)\|_2^2} (\mathbf{B}^b(t))^\times \boldsymbol{\tau}_{m,\text{ideal}} \quad (61)$$

Changing the angular momentum of the reaction wheels involves forcing the vector

$$\mathbf{h}_w = \mathbf{A} \mathbf{I}_s \boldsymbol{\omega}_s, \quad (62)$$

to zero. The wheels are slowed down by exerting wheel torques in the opposite of speed direction. For reaction wheel

attitude control systems with more than 3 wheels, the matrix $\mathbf{A} \mathbf{I}_s$ in (62) has a null space. That is, $\mathbf{A} \mathbf{I}_s \boldsymbol{\omega}_s$ is zero for other solutions than the trivial $\boldsymbol{\omega}_s = 0$. In particular when all wheels have equal inertia, the null space of (62) is given by

$$\boldsymbol{\omega}_s = c [1 \ 1 \ 1]^T, \quad \forall c \in \mathbb{R}, \quad (63)$$

indicating that while we are able to render the total angular momentum of the wheel system zero, the actual wheel speeds converge to a state in $\mathcal{N}(\mathbf{A} \mathbf{I}_s)$. To remedy this, we propose a procedure where we first control one wheel to zero. When this has been achieved we may use momentum dumping control laws proposed in the literature, for example in [23]:

$$\boldsymbol{\tau}^b = -\mathbf{A} \mathbf{I}_s \boldsymbol{\omega}_s. \quad (64)$$

We are now ready to give our momentum dumping scheme as the following procedure.

Step 1: Drive the speed of wheel 1 to zero while controlling the attitude with the remaining wheels, using the control law

$$\bar{\boldsymbol{\tau}}_a = -c \mathbf{B}_1 \boldsymbol{\omega}_s + \mathbf{B}_2 \boldsymbol{\tau}_a, \quad (65)$$

where $\mathbf{B}_1 = \text{diag}(1, 0, 0, 0)$, $\mathbf{B}_2 = \text{diag}(0, 1, 1, 1)$ and $\boldsymbol{\tau}_a$ is the normal control law.

Step 2: While retaining the modified control law (65), a torque is exerted by the magnetic torquers to dump momentum:

$$\boldsymbol{\tau}_{m,\text{ideal}}^b = -\mathbf{A} \mathbf{I}_s \boldsymbol{\omega}_s \quad (66)$$

which is implemented in magnetic moment using (61).

Step 3: When the wheel speed are sufficiently lowered, resume normal control $\boldsymbol{\tau}_a$ and turn off magnetic torquers.

Remark 3. *Due to the redundancy of the wheels, stability properties are not changed under the influence of the above control law. The three remaining wheels are able to exert the required torque for three-axis stabilization about all axes.*

VI. SIMULATIONS

In this section we present simulations of the observer, synchronizing controller and the momentum dumping scheme. The model used is based on realistic values for a cubic small-size satellite, and a summary of model parameters is given in Table I.

TABLE I
MODEL PARAMETERS

Parameter	Value
Inertia matrix	$\text{diag}\{4, 4, 3\} [kgm^2]$
Wheel inertia	$8 \cdot 10^{-3} [kgm^2]$
Max magnetic moment	40 [Am ²]
Max wheel torque	0.2 [Nm]
Max wheel speed	400 [rad/s]

TABLE II
SIMULATION PARAMETERS

Parameter	Value
Observer gains	$k_p = 400, k_v = 50$
Controller gains	$k_p = 1, k_d = 5$
Desired pointing accuracy	0.1° in all axes
Orbit angular velocity	$1.083 \cdot 10^{-3} \text{ [rad/s]}$
Initial attitude observer simulation	$[50, 50, 50]^T \text{ [Deg]}$
Initial leader attitude	$[0, 0, 0]^T \text{ [Deg]}$
Initial follower attitude	$[20, 20, 0]^T \text{ [Deg]}$

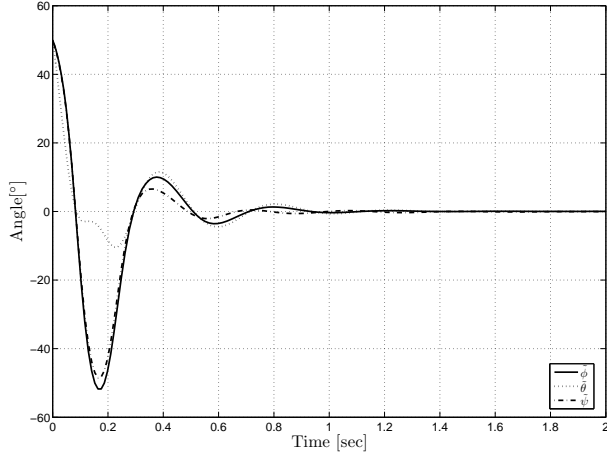


Fig. 3. Observer attitude error transient. Steady-state errors obtained were in the range of $\pm 0.02^\circ$

The observer was simulated in the presence of unmodelled torques and measurement noise, and a plot of the estimated attitude and velocity is presented in Fig. 3 and 4. The figures show the transient asymptotic behaviour. The steady-state error was in the order of $2 \cdot 10^{-2}^\circ$, but actual performance is dependent on the measurement equipment, actual unmodelled torques, noise, tuning parameters and so on.

In Fig. 5 a plot of the transient synchronization error is presented, clearly showing the asymptotic convergence. Steady-state error was in the order of .

The momentum dumping scheme was simulated on a satellite tracking a time-varying reference, where Step 1 was initiated at $t=500$ sec, Step 2 at $t=5000$ sec and finally Step 3 at $t=18000$ sec. Fig. 7 and 8 show how using our momentum dumping scheme, we are able to reduce both the total angular momentum of the wheel system *and* the individual wheel speeds. In addition Fig. 9 show that we are able to keep the control error within specified bounds, also during momentum management.

VII. CONCLUSION

We have in this paper presented the design of a synchronizing controller-observer scheme, including a momentum dumping procedure for the case of redundant wheels. The proposed controller was proved to be uniformly globally asymptotically stable using an extension of Matrosov's Theorem. Simulations have been utilized to support the propositions, showing that the control system performs to speci-

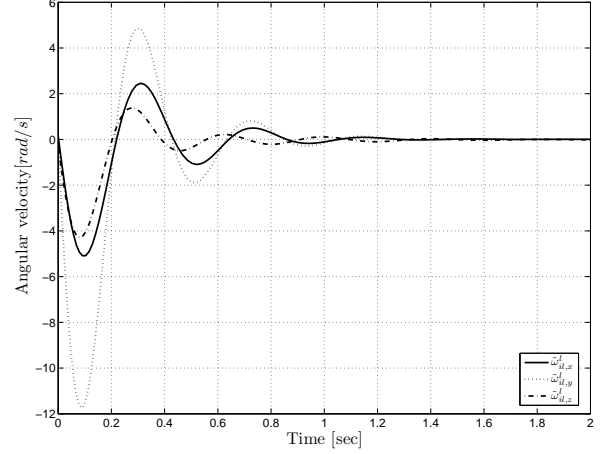


Fig. 4. Observer angular velocity error transient. Steady-state errors obtained were in the range of $\pm 5 \cdot 10^{-3} \text{ rad/s}$

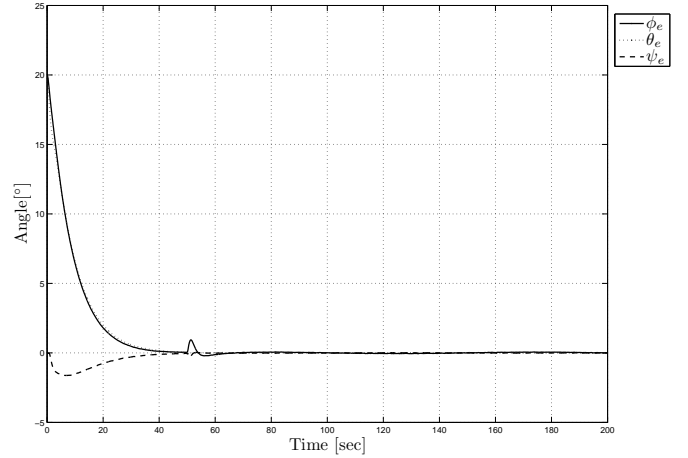


Fig. 5. Synchronization error transient \mathbf{q}_{se} , visualized in Euler angles.

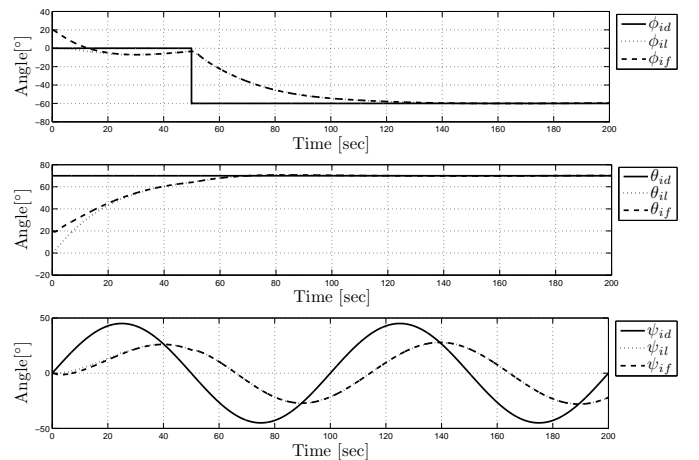


Fig. 6. Simulation plot showing the attitude of the leader and follower versus the desired attitude.

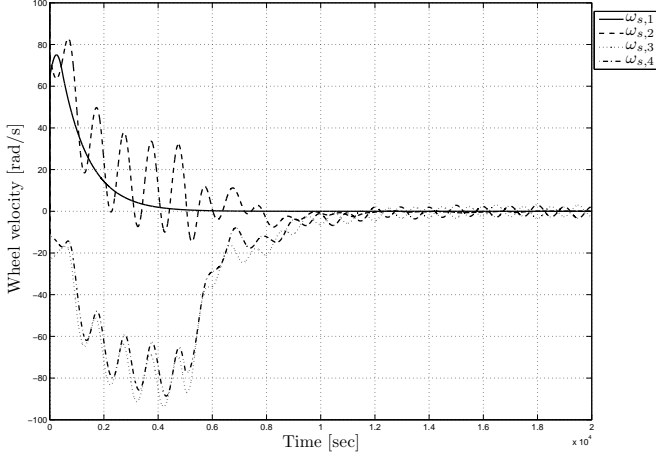


Fig. 7. Wheel speeds during momentum management.

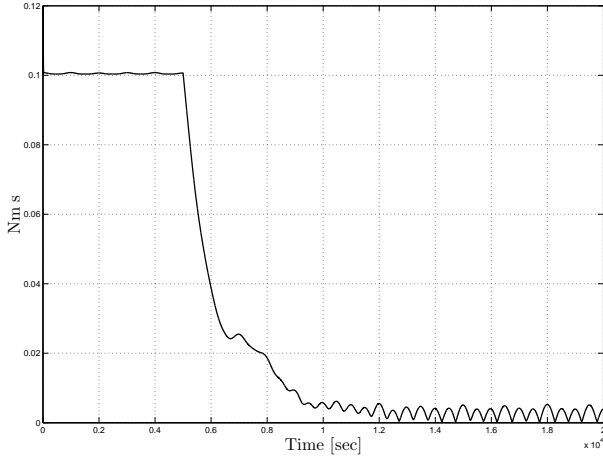


Fig. 8. Two-norm of the total angular momentum, $\|\mathbf{h}_w\|_2$.

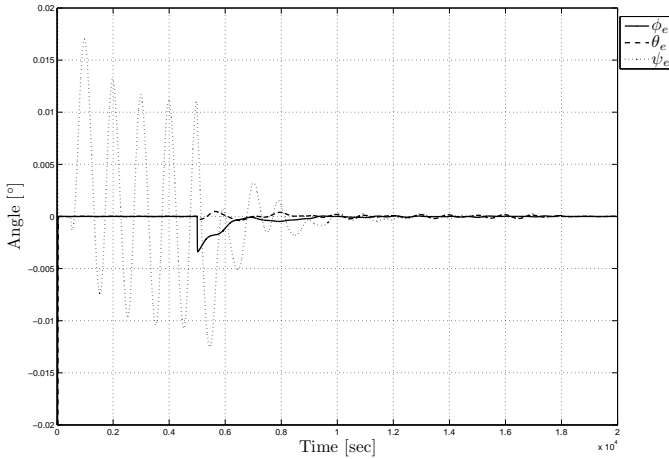


Fig. 9. Attitude tracking error, during momentum management.

fications also when no velocity measurements are available and environmental disturbances are included.

APPENDIX

A. Stability theorems

In this section we give some theorems used in the proofs of our propositions. The theorems are given for the general nonlinear non-autonomous system

$$\dot{x} = f(t, x) \quad (67)$$

Theorem 1 (Uniform stability [24]). *Let $x = 0$ be an equilibrium point for (67) and $\mathbb{D} \subset \mathbb{R}^n$ be a domain containing $x = 0$. Let $V : \mathbb{R}_{\geq 0} \times \mathbb{D} \rightarrow \mathbb{R}$ be a continuously differentiable function such that*

$$W_1(x) \leq V(t, x) \leq W_2(x) \quad (68)$$

$$\frac{\partial V}{\partial t} + \frac{\partial V}{\partial x} f(t, x) \leq 0 \quad (69)$$

$\forall t \geq 0$ and $\forall x \in \mathbb{D}$, where $W_1(x)$ and $W_2(x)$ are continuous positive definite functions on \mathbb{D} . Then, $x = 0$ is uniformly stable. If $\mathbb{D} = \mathbb{R}^n$, then $x = 0$ is uniformly globally stable (UGS).

Theorem 2 (Extension of Matrosov's Theorem, [12], [13]). *Under the following assumptions, the origin of the system (67) is UGAS.*

Assumption 1. *The origin of the system (67) is UGS.*

Assumption 2. *There exist integers $j, m > 0$ and for each $\Delta > 0$ there exist*

- a number $\mu > 0$
- locally Lipschitz continuous functions $V_i : \mathbb{R} \times \mathbb{R}^n \rightarrow \mathbb{R}, i \in \{1, \dots, m\}$
- a (continuous) function $\phi : \mathbb{R} \times \mathbb{R}^n \rightarrow \mathbb{R}^m, i \in \{1, \dots, m\}$
- continuous functions $Y_i : \mathbb{R}^n \times \mathbb{R}^m \rightarrow \mathbb{R}, i \in \{1, \dots, j\}$

such that, for almost all $(t, x) \in \mathbb{R} \times \mathcal{B}(\Delta)^1$,

$$\max\{|V_i(t, x)|, |\phi(t, x)|\} \leq \mu, \quad (70)$$

$$\dot{V}_i(t, x) \leq Y_i(x, \phi(t, x)). \quad (71)$$

Assumption 3. *For each integer $k \in \{1, \dots, j\}$ we have that*

$$\{(z, \psi) \in \mathcal{B}(\Delta) \times \mathcal{B}(\mu), Y_i(z, \psi) = 0 \quad (72)$$

$$\forall i \in \{1, \dots, k-1\}\} \Rightarrow \{Y_k(z, \psi) \leq 0\}. \quad (73)$$

Assumption 4. *We have that*

$$\{(z, \psi) \in \mathcal{B}(\Delta) \times \mathcal{B}(\mu), Y_i(z, \psi) = 0 \quad (74)$$

$$\forall i \in \{1, \dots, j\}\} \Rightarrow \{z = 0\}. \quad (75)$$

Proof. See [13]. □

¹ $\mathcal{B}(\Delta) = \{x \in \mathbb{R}^n \mid \|x\| \leq \Delta\}$

REFERENCES

- [1] H. Pan and V. Kapila. Adaptive nonlinear control for spacecraft formation flying with coupled translational and attitude dynamics. In *Proceedings of the 40th IEEE Conference on Decision and Control*, 2001.
- [2] W. Kang and H. Yeh. Co-ordinated attitude control of multi-satellite systems. *International Journal of Robust and Nonlinear Control*, 12:185–205, 2002.
- [3] P.K.C Wang, F.Y. Hadaegh, and K. Lau. Synchronized formation rotation and attitude control of multiple free-flying spacecraft. *Journal of Guidance, Control and Dynamics*, pages 28–35, 1999.
- [4] H. Nijmeijer and A. Rodriguez-Angeles. *Synchronization of Mechanical Systems*. World Scientific, 2003.
- [5] M.J. Mataric. Minimizing complexity in controlling a mobile robot population. In *1992 IEEE Int. Conf. on Robotics and Automation Proceedings*, volume 1, pages 830–835, May 1992.
- [6] T. Balch and R.C. Arkin. Behavior-based formation control for multirobot teams. *IEEE Transactions on Robotics and Automation*, 14(6), December 1998.
- [7] A. D. Mali. On the behavior-based architectures of autonomous agency. *IEEE Transactions on Systems, Man and Cybernetics, Part C: Applications and Reviews*, 32(3), August 2002.
- [8] J.R.T. Lawton. *A Behavior-Based Approach to Multiple Spacecraft Formation Flying*. PhD thesis, Brigham Young University, Dept. of El. and Comp. Engineering, November 2000.
- [9] M.A. Lewis and K. Tan. High precision formation control of mobile robots using virtual structures. *Autonomous Robots*, 4:pp. 387–403, 1997.
- [10] R.W. Beard, J. Lawton, and F.Y. Hadaegh. A coordination architecture for formation control. *IEEE Transactions on Control Systems Technology*, 9:pp. 777–790, 2001.
- [11] W. Ren and R.W. Beard. Formation feedback control for multiple spacecraft via virtual structures. In *2004 IEEE Proceedings of Control Theory Application*, 2004.
- [12] V. M. Matrosov. On the stability of motion. *Journal of Appl. Math. Mech.*, 26:pp. 1337–1353, 1962.
- [13] A. Loria, E. Panteley, D. Popovic, and A.R. Teel. An extension of matrosov’s theorem with application to stabilization of nonholonomic control systems. In *Proceedings of the 41st IEEE Conference on Decision and Control*, volume 2, pages pp. 1528–1533, December 2002.
- [14] H. Nijmeijer, I.L. Blekhman, A.L. Fradkov, and A.Yu. Pogromsky. Self-synchronization and controlled synchronization. *Proceedings of 1st International Conference on Control of Oscillations and Chaos*, 1:36–41, 1997.
- [15] E. Kyrkjebø and K.Y. Pettersen. Ship replenishment using synchronization control. In *Proc. 6th Conference on Manoeuvring and Control of Marine Crafts*, 2003.
- [16] R. Wisniewski. Lecture notes on modeling of a spacecraft. [Available online: www.control.auc.dk/~raf/ModellingOfMech/Rep8sem.ps, Last accessed: 05.06.2005], May 2000.
- [17] Peter C. Hughes. *Spacecraft attitude dynamics*. John Wiley & Sons, 1986.
- [18] O. Egeland and J.T. Gravdahl. *Modeling and Simulation for Automatic Control*. Marine Cybernetics, 2001.
- [19] O.-E. Fjellstad. *Control of unmanned underwater vehicles in six degrees of freedom*. PhD thesis, Norwegian University of Science and Technology, 1994.
- [20] B. O. Sunde. Satellite attitude determination. Master’s thesis, Department of Engineering Cybernetics, Norwegian University of Science and Technology, 2005.
- [21] C. Arduni and P. Baiocco. Active magnetic damping attitude control for gravity gradient stabilized spacecraft. *Journal of Guidance, Control and Dynamics*, 20(1):pp. 117–122, January-February 1997.
- [22] M. Lovera and A. Astolfi. Spacecraft attitude control using magnetic actuators. *Automatica*, 20:pp. 1405–1414, 2004.
- [23] Marcel J. Sidi. *Spacecraft Dynamics & Control: A Practical Engineering Approach*. Cambridge, 1997.
- [24] H.K. Khalil. *Nonlinear Systems*. Prentice Hall, 3 edition, 2000.